Life Sciences xxx (xxxx) 120403

Contents lists available at ScienceDirect

Life Sciences

journal homepage: www.elsevier.com/locate/lifescie

PEG-4000 formed polymeric nanoparticles loaded with cetuximab downregulate *p21* & *stathmin-1* gene expression in cancer cell lines

Ahmed A. H. Abdellatif PhD [a, b, *], Nahla Sameh Tolba [c], Mansour Alsharidah [d], Osamah Al Rugaie [e], Abdellatif Bouazzaoui [f, g, h], Imran Saleem [i], Asmaa T. Ali [j]

[a] Department of Pharmaceutics, College of Pharmacy, Qassim University, Qassim 51452, Saudi Arabia
[b] Department of Pharmaceutics and Pharmaceutical Technology, Faculty of Pharmacy, Al-Azhar University, Assiut 71524, Egypt
[c] Department of Pharmaceutics, Faculty of Pharmacy, Sadat City University, Monufia 32897, Egypt
[d] Department of Physiology, College of Medicine, Qassim University, Buraydah 51452, Saudi Arabia
[e] Department of Basic Medical Sciences, College of Medicine and Medical Sciences, Qassim University, Unaizah, P.O. Box 991, Al Qassim 51911, Saudi Arabia
[f] Department of Medical Genetics, Faculty of Medicine, Umm Al-Qura University, Makkah 21955, Saudi Arabia
[g] Science and Technology Unit, Umm Al-Qura University, Makkah 21955, Saudi Arabia.
[h] Medical Clinic, Hematology/Oncology, University Hospital Regensburg, Franz-Josef-Strauß-Allee 11, Regensburg 93053, Germany
[i] School of Pharmacy & Biomolecular Sciences, Liverpool John Moores University, James Parsons Building, Liverpool L3 3AF, UK
[j] Department of Biochemistry, Faculty of Pharmacy, Nahda University, Beni-Suef 62513, Egypt

ARTICLE INFO

Keywords:
Cetuximab
Polymeric nanoparticles
A549 lung cancer cell line
MCF-7 breast cancer cell line
Stathmin-1
Gene expression and regulation

ABSTRACT

Cetuximab (CTX) is known to have cytotoxic effects on several human cancer cells *in vitro*; however, as CTX is poorly water soluble, there is a need for improved formulations can reach cancer cells at high concentrations with low side effects. We developed (PEG-4000) polymeric nanoparticles (PEGNPs) loaded with CTX and evaluated their *in vitro* cytotoxicity and anticancer properties against human lung (A549) and breast (MCF-7) cancer cells. CTX-PEGNPs were formulated using the solvent evaporation technique, and their morphological properties were evaluated. Further, the effects of CTX-PEGNPs on cell viability using the MTT assay and perform gene expression analysis, DNA fragmentation measurements, and the comet assay. CTX-PEGNP showed uniformly dispersed NPs of nano-size range (253.7 ± 0.3 nm), and low polydispersity index (0.16) indicating the stability and uniformity of NPs. Further, the zeta potential of the preparations was −17.0 ± 1.8 mv. DSC and FTIR confirmed the entrapping of CTX in NPs. The results showed IC_{50} values of 2.26 μg/mL and 1.83 μg/mL for free CTX and CTX-PEGNPs on the A549 cancer cell line, respectively. Moreover, CTX-PEGNPs had a lower IC_{50} of 1.12 μg/mL in MCF-7 cells than that of free CTX (2.28 μg/mL). The expression levels of *p21* and *stathmin-1* were significantly decreased in both cell lines treated with CTX-PEGNPs compared to CTX alone. The CTX-PEGNP-treated cells also showed increased DNA fragmentation rates in both cancer cell lines compared with CTX alone. The results indicated that CTX-PEGNP was an improved formulation than CTX alone to induce apoptosis and DNA damage and inhibit cell proliferation through the downregulation of *P21* and *stathmin-1* expression.

1. Introduction

Human cancers are usually associated with abnormal overexpression of the epidermal growth factor receptor (EGFR); therefore, anti-EGFR drugs are suitable candidates for treating different types of cancer, including lung and breast cancers [1,2]. Cetuximab (CTX) is a clinically available recombinant chimeric human/mouse IgG1 anti-EGFR monoclonal antibody that binds to the extracellular domain of EGFR and prevents it from activating downstream signaling pathways such as of cell proliferation, invasion, metastasis, and neovascularization [3,4]. Inhibition of receptor phosphorylation and activation of receptor-associated kinases can also block receptor-dependent transduction pathways and promote antitumor effects, which include cell cycle arrest, apoptosis induction, and inhibition of angiogenesis [5]. CTX has recently been shown to have promising anticancer activity in preclinical investigations, both alone and in combination with established cyto-

(CTX), Cetuximab; (PEG), polyethylene glycol; (PEGNPs), Polymeric nanoparticles; CTX-PEGNPs, Cetuximab loaded polymeric nanoparticles

* Corresponding author at: College of Pharmacy, Qassim University, Saudi Arabia.
E-mail addresses: a.abdellatif@qu.edu.sa (A.A.H. Abdellatif), nahla.sameh@fop.usc.edu.eg (N.S. Tolba), malsharidah@qu.edu.sa (M. Alsharidah), o.alrugaie@qu.edu.sa (O. Al Rugaie), alazzauoi@uqu.edu.sa (A. Bouazzaoui), i.saleem@ljmu.ac.uk (I. Saleem), asmaa.tarek@nub.edu.eg (A.T. Ali).

https://doi.org/10.1016/j.lfs.2022.120403
Received 19 December 2021; Received in revised form 5 February 2022; Accepted 10 February 2022

toxic drugs, and has been widely recommended and shown to be useful for breast cancer treatment [6].

CTX is poorly soluble in water, which limits its bioavailability. Moreover, coating CTX can improve its cell penetration and targeting at the site of action. Coating CTX with polyethylene glycol (PEG) can enhance its water solubility and concentration at the absorption site [7]. Polymeric nanoparticles (PEGNPs) can be loaded with active ingredients that are either entrapped within the polymeric core or adsorbed on its surface. The advantage of using PEGNPs is that the carriers keep the drugs and additional biologically active fragments protected from the environment and increase the bioavailability and therapeutic index of the drugs [8,9]. It was reported that a coumarin-dihydropyrimidinone formulated in poly(lactic-*co*-glycolic acid) (PLGA)-PEG_{4000} mixed copolymer nanoparticles showed excellent therapeutic effect on a wide variability of cancer cell lines [10].

Polyethylene glycol (PEG) is commonly used in medicine delivery and nanotechnology because to its biocompatibility and "stealth" qualities. PEGylation is considered to help particle delivery systems and hence extend circulation lifetimes [11]. PEGylation increases circulatory half-life but not protein binding [12,13]. Moreover, PEG especially PEG-4000 is freely water soluble and ethanol soluble [14]. The solubility of the incorporated drugs in PEG-4000 is increased, as PEG-4000 is considered as a surfactant [15]. The covalent bonding of PEG to a medication or therapeutic protein might "cover" the agent from the host's immune system (so decreasing immunogenicity and antigenicity) and increase its hydrodynamic size (size in solution), thereby prolonging its circulation duration by decreasing renal clearance [16].

p21 is a well-known WAF1/CIP1 (activating factor/cyclin-dependent kinase inhibitory protein-1) that was found to be vital for modulating cell cycle progression [17,18]. Early research on non-small cell lung cancer (NSCLC) revealed that in well-differentiated tumors, *p21* is overexpressed [19] and stimulates tumor growth suppression via p53 activity, consistent with its cell cycle arrest activity [20]. Nevertheless, other studies have suggested that some pathways are not dependent on p53 and lead to *p21* induction [20]. These investigations have focused on inducing *p21* in p53-deficient cancer cells in which the G1 checkpoint and cell cycle arrest could be triggered [20]. Besides cell cycle arrest, *p21* is involved in apoptosis via p53-dependent and p53-independent processes. *p21* is similarly involved in regulating several cellular activities, including actin cytoskeleton reorganization, apoptosis, and DNA damage response [21]. Hence, the induction of *p21* has been demonstrated to be critical for the mobility of cancer cells and carcinogenesis. As a result, *p21* has a dual function in cancer depending on whether it is found in the cytoplasm or the nucleus. It can function as an oncogene or a tumor suppressor protein.

Understanding how malignant tumors work at a cellular level is critical for identifying novel treatments. Statistics show that *stathmin-1* is overexpressed in many human malignant tumors, which may promote malignant cell development and growth. The stathmin-1 family of microtubule-regulating proteins includes stathmin-1, SCG10, SCLIP, and RB3/RB3'/RB3" [22]. These members of the stathmin-1 family harbor a conserved domain with a tubulin-binding activity. In malignant tumors, stathmin-1 depletion inhibits cell proliferation, motility, and metastasis and induces apoptosis [23]. *Stathmin-1* may be a promising therapeutic target because it inhibits multiple aspects of tumor progression. In addition to regulating cell proliferation, differentiation, and function, *stathmin-1*, a small regulatory protein, presumably integrates several intracellular signaling pathways. Downstream target or partner proteins interact with *stathmin-1* to produce biological effects via *stathmin-1* phosphorylation [24]. Several studies have examined the expression of *stathmin-1* and showed that the expression is linked to several malignant cancers, including lung, breast, and esophageal cancers [25–28].

In this study, we formulated CTX-PEGNPs using PEG-4000 as a novel formulation for the first time, to the best of our knowledge. We formulated CTX-PEGNPs with improved water solubility and the ability to deliver the drug at cancer sites. CTX-PEGNPs were evaluated for their *in vitro* cytotoxicity and anticancer properties against human lung (A549) and breast (MCF-7) cancer cells. CTX-PEGNPs were formulated using the solvent evaporation technique, and their morphological properties were evaluated. CTX-PEGNPs were used to probe the molecular expression of *stathmin-1,* which controls tumor cell growth, death, and migration. These NPs are a promising tool for investigating the molecular effects of lung and breast cancer treatments *in vitro,* and we demonstrated the cytotoxic effects and induction of DNA damage in A549 and MCF-7 cancer cell lines. Furthermore, we focused on targeting *p21* in the A549 lung cancer cell line. The study findings suggest that CTX-PEGNPs are an effective anticancer agent for different tumor cell types.

2. Materials and methods

2.1. Materials, media and reagents

CTX, methanol, glycerol, polyethene glycol (PEG) 4000, SYBR® Premix Ex TaqTM, and reconstituted vials of MTT (M-5655) were obtained from Sigma-Aldrich Chemie GmbH (Eschenstrasse, Taufkirchen, Germany). Chloroform and Tween 80 were purchased from El Gomhouria Co. (Cairo, Egypt). The RNeasy Mini Kit and DNase I were procured from Qiagen, Hilden, Germany, whereas RNAse-free DNAse, the RevertAidTM First Strand cDNA Synthesis Kit, and agarose were purchased from Thermo Fisher Scientific, Waltham, MA, USA. These were used for RNA extraction and cDNA synthesis from lung and breast cancer cell lines. Gene expression was quantified using the StepOne™ Real-Time PCR System from Applied Biosystems (Waltham, MA, USA). The A549 and MCF-7 cell lines were acquired from the American Type Culture Collection (ATCC, Manassas, VA, USA). Gibco's Dulbecco's Modified Eagle Medium (DMEM), penicillin-streptomycin, and fetal bovine serum (FBS; Hyclone, Salt Lake City, UT, USA) were used for cell culture.

2.2. Preparation CTX-PEGNPs polymeric nanoparticle

The CTX-PEGNPs containing 100 pmol CTX were prepared using the solvent evaporation method as previously described [9,29] with some modifications. In brief, 1 mg CTX was dissolved in 5 mL methanol: chloroform (1,1) mixture, and the mixture was then added to the aqueous phase made of 40 mL water, 1 mL Tween-80, and 10 mL glycerol. The PEG-4000 polymer was dissolved in the aqueous phase at a drug-polymer ratio of 1:1. The organic phase was dropped into the aqueous phase at a rate of 2 mL every 10 min and homogenized using a homogenizer for 10 min at 12,000 rpm (Ultra Turrax; IKA Labortechnik, Staufen, Germany). The solution was subsequently stirred on a magnetic stirrer to allow the organic solvent to evaporate. The resulting mixture was then centrifuged (Avanti centrifuge J-E/ Beckman coulter GmbH, Germany) at 5000 rpm for 5 min to separate the polymeric NPs from any non-reacting molecules that may have been included in the solution.

2.3. Solubility and dissolution studies

The solubility and dissolution of CTX were determined in distilled phosphate buffer (0.1 M) (pH 7.4) at 37.5 °C. The dissolution of CTX and CTX-PNs in phosphate buffer were used also as indication of improved solubility. In a dissolution tester (Validata–Hansen study Chatsworth, Ca, USA), an aliquot of CTX, and CTX-PNs to 5 mg drug rotated at 50 rpm. 1 mL of sample was withdrawn and substituted by 1 mL of phosphate buffer at predefined 0-200 min [30]. After equilibrium of solution, aliquots were collected, filtered through a 0.45 μm membrane filter, and quantified using a spectrophotometer (Genesis 10 UV, Thermo Electron Corporation, USA) at λ_{max} 280 nm. Moreover, the re-

lease model, the release pattern of the CTX, and CTX-PNs were described. The release data of the prepared formulae were analyzed according to zero order, first order, Higuchi diffusion, and Hixson Crowell equation [7]. *Zero order equation ($Q_t = Q_0 - K_0t$), 1st order equation (log Q_t = log Q_0 - K_1t/ 2.303), Higuchi's equation ($Q_t = K_h\sqrt{t}$), and Hixson Crowell equation $M^{1/3} - M_t^{1/3} = K_t$.* Where Q_t denotes the amount of medication released at time t, K denotes the release rate constant, and n denotes the type of release mechanism used throughout the dissolution process. M_0 is the initial amount of drug in the formula. M_t is the remaining amount of drug in the formula at a time `t' and K is proportionality constant. Burnham and Anderson advised that the most appropriate model be chosen based on the correlation coefficient (r) for the parameters involved and the diffusional exponent's values (n).

2.4. Evaluation of particle size, polydispersity index, and zeta potential

A dynamic light scattering, Zetasizer (Malvern Instruments GmbH, Herrenberg, Germany) was used to determine the size and polydispersity index (PDI) of CTX-PEGNPs. 1 mL of diluted NPs suspension was vortexed for 5 min before being placed in a Zetasizer cell. The Zetasizer was also used to determine the zeta potential using photon correlation spectroscopy as previously described [31].

2.5. Entrapment efficiency

To determine the quantity of CTX entrapped in PEGNPs, the NPs were centrifuged (Avanti centrifuge J-E/Beckman coulter GmbH, Germany) at 15,000 rpm for 15 min. A 5 mL aliquot of the supernatant was combined with 5 mL of methanol-chloroform solution (1:1). The amount of CTX was measured using a single-beam UV spectrophotometer at λ_{max} 280 nm (Genesis 10 UV, Thermo Electron Corporation, USA) against a methanol-chloroform blank solution. Eq. (1) was used to calculate the drug concentration. Each batch experiment was repeated three times to determine and record the average.

$$EE\% = \frac{\text{Total drug added–the amount of free drug}}{\text{total drug added}} \times 100 \quad (1)$$

2.6. Morphological study by transmission electron microscopy

The external morphology of the NPs was examined by transmission electron microscopy (TEM; JEOL 100CX; JEOL Inc., Peabody, MA, USA) at an accelerating voltage of 80 kV. The CTX-PEGNP formula was diluted from 1% to 0.01% *w/v* and treated in an ultrasonic bath for 1 h using (Model 3510, Branson, MS) to reduce particle aggregation on the copper grid. One drop of the NP formula was applied to a carbon-coated copper grid and dried for TEM testing [32]. The distribution of CTX-PEGNP dimensions was evaluated from TEM images using Image J version 1.45 k [33].

2.7. Differential scanning calorimetry (DSC)

Differential Scanning Calorimetric was applied (Setaram instrument version Themys one$^+$, Switzerland) to investigate any possible interactions between CTX, PEG 4000 and Glycerol [34]. Generally, DSC measures the temperatures and heat flows associated with transitions in materials as a function of time and temperature range (- 4.9 to 489.9 °C) in a controlled atmosphere. The samples were enclosed in a heat flux DSC, the CTX-PNs were used as a liquid form and then were enclosed in pan. Moreover, an empty reference pan was placed on a thermoelectric disk. A small amount of sample (from 2 to 5 mL) were added on the pan and let it dry overnight before running the DSC process. The samples (from 2 to 5 mg) were heated under nitrogen with rate of 10 °C/min and if any kind of transition takes place during this process lead to a slight difference between the sample and a reference sample temperature, i.e. differential scanning calorimetry measures the amount of energy (heat) absorbed or released by a sample as it is heated, cooled, or held at a constant temperature [35].

2.8. Fourier-transform infrared spectroscopy (FTIR)

FTIR was used to verify the compatibility of all tested components together. We intended to detect any drug interactions between the drug and polymer by collecting data between 400 and 4000 cm^{-1} of data from each component. CTX-PNs were compared with the raw materials data, and mixture of CTX powder, PEG-4000, and glycerol which were subjected to FTIR (Resolution 4 cm^{-1}, scan number 100), Spectrophotometer Thermo Nicolet Nexus (Thermo, Bremen, Germany) [36,37].

2.9. Cell culture

Both A549 and MCF-7 cell lines were cultured under standard conditions as reported previously [38] using DMEM (10% FBS), 10 μg/mL insulin, and 1% penicillin-streptomycin. The cells were seeded at a density of 1.2–1.8 × 10^3 cells/well in 100 μL complete growth medium + 100 μL of each sample/well in a 96-well plate for 24 h at 37 °C before the MTT assay. Stock cells were grown in DMEM (10% inactivated FBS, 100 IU/mL penicillin, 100 mg/mL streptomycin, and 5 mg/mL amphotericin B) at 37 °C and 5% CO_2 until confluent. The cells were dissociated using a solution of trypsin phosphate versene glucose (trypsin 0.2%, ethylene diamine tetraacetic acid [EDTA] 0.02%, and glucose 0.05% in phosphate-buffered saline). Stock cultures were established in 25 cm^2 culture flasks, and all experiments were performed in 96-well microtiter plates [39,40].

2.10. MTT cytotoxicity assay

The cytotoxic effect of free CTX drug application and CTX-PEGNPs on A549 and MCF-7 cells was studied after 48 h using a standard MTT assay as reported previously [41]. Cells in the log growth phase were used at a final cell density of 1 × 10^6 cells/cm^2. Each test included a blank containing cell-free complete medium. Each vial of MTT [M-5655] was reconstituted with 3 mL of medium or balanced salt solution without phenol red and serum. The reconstructed MTT was added as 10% of the culture medium volume and incubated for 2 h. The resultant formazan crystals were dissolved by adding an MTT solubilization solution [M-8910] in a volume equivalent to that of the original culture medium. The absorbance at 570 nm was used spectrophotometrically to determine cytotoxicity.

2.11. Gene expression analysis

The RNeasy Mini Kit supplemented with a DNase I digestion step was used to isolate total RNA from lung and breast cancer cell lines according to the manufacturer's instructions. The quantitative real-time PCR (qPCR) reactions were set up in 25 μL reaction mixtures containing 12.5 μL 1× SYBR® Premix Ex TaqTM, 0.5 μL of each primer at a concentration of 0.2 μM, 6.5 μL distilled water, and 5 μL cDNA template. The PCR reaction was set up as follows: initial denaturation, 3 min at 95.0 °C; 40 cycles of denaturation, 15 s at 95.0 °C; annealing, 30 s at 55.0 °C; extension, 30 s at 72.0 °C; and a final step of 71 cycles that began at 60.0 °C, and the temperature rose by approximately 0.5 °C every 10 s until the temperature reached 95.0 °C. At the conclusion of each RT-qPCR, a melting curve analysis at 95.0 °C was conducted to determine the quality of the primers used. A distilled water control was included in each experiment. The sequences of specific primers for lung (*p21* and *CDKN1A*) and breast (*stath*min-*1* and *α-tubulin*) cancer-related genes are listed in Table 1. The $2^{-\Delta\Delta CT}$ approach was used to determine the relative quantification of the target to the reference [42].

Table 1
Primer sequences used for *RT-qPCR* of lung and breast cancer cell lines.

Gene	Forward	GenBank accession no
p21	F: CCTGTGTGTGTTTGCCATCA	J00277.1
	R: TGAGAGGTGGAAAGCGAGAG	
stathmin	F: GTCTTCCAGAGTCACACCCA	NM_001276310.2
	R: TGAGTCCCACAAAAGCCAGA	
β-actin	F: CATGGAATCCTGTGGCATCC	HQ154074.1
	R: CACACAGAGTACTTGCGCTC	

p21: protein 21; *CDKN1A*: cyclin dependent kinase inhibitor 1A.

2.12. DNA damage measurement using the comet assay

DNA damage in lung and breast cancer cell lines was determined using the comet assay [43]. The cultured cells were treated with trypsin to produce single-cell suspensions. In total, 1.5×10^4 cells were embedded in 0.75% low melting temperature agarose and quickly pipetted onto a pre-coated microscope slide. The embedded cells were lysed in 0.5% sodium dodecyl sulfate and 30 mM EDTA, pH 8.0, for 50 min at 4 °C. After rinsing in Tris-borate-EDTA buffer (pH 8.0) overnight at 37 °C, the lysed cells were subjected to electrophoresis at 0.6 V/cm for 25 min. Subsequently, the lysed cells were stained with propidium iodide. A fluorescent microscope (BioTek, Winooski, Vermont, USA) with a CCD camera was used to examine the slides. For each sample, approximately 100 cells were examined to determine the percentage of cells with DNA damage that appear like comets. Based on perceived comet tail length m, non-overlapping cells were randomly selected and scored on an arbitrary scale of 0 to 3 (class 0 = no detectable DNA damage and no tail; class 1 = tail with a length less than the diameter of the nucleus; class 2 = tail with a length between 1 and 2 times the nuclear diameter; and class 3 = tail longer than 2 times the diameter of the nucleus) [44].

2.13. DNA fragmentation assay

The DNA fragmentation in lung and breast cancer cell lines was measured following the method established by Yawata et al. [45] with some modifications. Briefly, lung and breast cancer cell lines were exposed to test substances for 24 h in different Petri dishes (60 × 15 mm, Greiner). The cells were then trypsinized and collected (including floating cells), which were then washed with Dulbecco's phosphate-buffered saline. Further, the cells were lysed using 150 mM NaCl, 10 mM Tris (pH 7.4), 5 mM EDTA, and 0.5% Triton X-100 for 30 min on ice. The lysates were clarified by vortexing and centrifuging at 10,000 ×g for 20 min. Fragmented DNA was recovered from the supernatant using an equal amount of a neutral phenol:chloroform:isoamyl alcohol solution (25:24:1) and electrophoretically separated on 2% agarose gels containing 0.1 μg/mL ethidium bromide.

2.14. Statistical analysis

The data are reported as the mean of at least three experiments with the standard deviation. SPSS Statistics was used to compute one-sample or two-sample *t*-tests (IBM). $*p \leq 0.05$, $**p \leq 0.01$ or $***p \leq 0.001$ denote statistically significant differences.

3. Results and discussion

3.1. Evaluation of solubility, release, particle size, polydispersity index, and zeta potential

The CTX powder showed full release after 150 min, while the CTX was released from CTX-PNs after 13 min which reflect the improvement of CTX solubility released from NPs (Fig. 1A). From Table 2:, the release of drug from formulation CTX-PNs followed zero order kinetics with r^2 equal to 0.878 and that the mechanism of release was dissolution controlled according to Hixson-Crowell equation with r^2 equal to 0.957. From the other hand the release of drug from formulation CTX followed zero order kinetics with r^2 equal to 0.883 and the mechanism of release was diffusion controlled according to Higuchi equation with r^2 equal to 0.976 (Table 2:). Comparing the drug release and solubility from free CTX and CTX loaded PEGNPs, the PEG-4000 significantly enhanced the release profile of the CTX from PEGNPs, These results showed that CTX were completely dissolved after 13 min in phosphate medium, which justifies the role of PEG-4000 as a coat that can significantly increase solubility and enhance the targeting of CTX to its site. These results are agreed with that published by El-Badry et al. [46], who showed an improve of solubility and dissolution rate of indomethacin by PEG4000. Also, we used this formulae depending on our previously work published work [9].

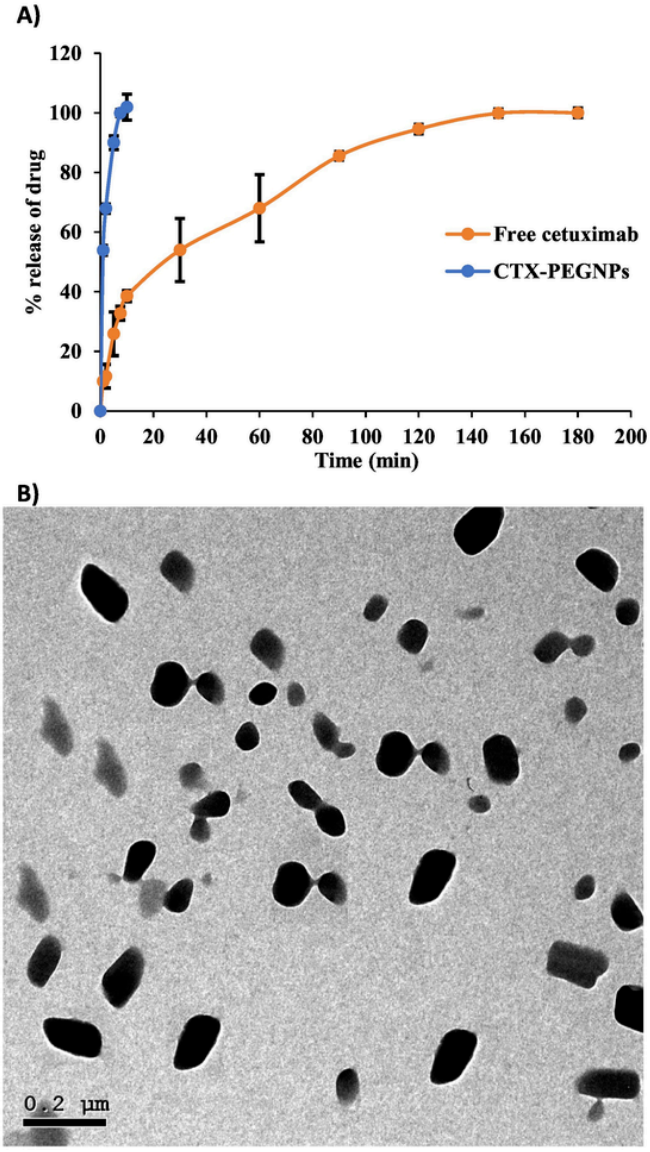

Fig. 1. (A) CTX-PEGNP solubility study and dissolution rate in phosphate buffer pH 7.4, the samples were measured in triplicate (±SD), and (B) TEM micrograph of a single particle size.

The particle size of CTX-PEGNPs was found to be 253.7 ± 0.3 nm (**S**. 1A). These results were similar to that obtained by Sabra et al., [47]. The PDI is a dimensionless and scaled parameter that is an indicator of homogeneity. The PDI of the CTX-PEGNP formula was 0.168 ± 0.1, which indicated good homogeneity, as a PDI value close to 0 suggests

that the dispersion is homogeneous, whereas a value greater than 0.3 indicates high heterogeneity [48]. It was reported, a sample with an extremely broad size distribution and a PDI of >0.7 is most likely unsuitable for dynamic light scattering (DLS) [49]. The surface properties and stability of the nanosuspensions were investigated using zeta potential analysis. The zeta potential of the preparations was −17.0 ± 1.8 mv (**S.** 1B), which indicated that the system was sufficiently stable. NPs with zeta potentials between −10 and + 10 mV are neutral, but NPs with zeta potentials greater than +10 mV or lesser than −10 mV are strongly cationic or strongly anionic, respectively [49].

This size is not considered the optimum size for cell membrane internalization. However, these sizes can penetrate the cell membrane efficiently. Several studies have shown that NPs internalized well when smaller than 50 nm, while the NPs uptake decreased for smaller (15–30 nm) and bigger (70–240 nm) particles [50]. This size is considered larger size which could be internalized by phagocytosis. Phagocytosis is the process of specialized mammalian cells called phagocytes taking up detritus, germs, or other large solutes [51]. Studies show that a smaller microsphere can attach to cells faster and stronger. [52,53]. Other studies have demonstrated that particles of smaller size directly contribute to the rapid internalization of particles by cells [54]. When compared to spherical particles, microrod particles were more successful in inducing non-specific cellular uptake, as seen by higher apoptotic signal and proliferation inhibition, as well as increased apoptosis [55]. Following endocytosis, it has been observed that various particles spatially segregate in the cytoplasm depending on their size and shape [56]. A study using spheres and elliptical disks of varied sizes (0.1–10 m) and forms (spheres vs. elliptical disks) suggests that spheres were endocytosed more swiftly, whereas disks circulated longer in the blood with a greater targeting specificity in mice [55,57].

3.2. The entrapment efficiency

The percent entrapment efficiency (EE%) indicates the amount of drug that can be entrapped in the polymer matrix in the dispersed state, which describes the drug miscibility limit in the polymer. Due to the poor solubility of CTX in the external aqueous phase, reasonable EE% values were obtained for the prepared NPs which found to be 60.5 ± 1.3%. CTX is practically insoluble in distilled water and phosphate buffer (pH 7.4) at 37.5 °C. The enhanced solubility of CTX can be explained by the adjustment of the nano-formulation of CTX in polymeric NPs. These results agree with those of Ranneh et al. who used surfactants to improve the solubility and stability of a water-insoluble anticancer medication in liquid crystalline-phase NPs due to NP formation [58]. In addition, the EE% were similar with that obtained by Abdellatif et al., [7] who obtained maximum entrapment of CTX in a sodium alginate polymer between 40% and 65%. There is no limit to EE%, as it usually depends on drug solubility (the soluble drug has the low EE% and vice versa). Also, depend on the polymer ratios, the higher polymer ratio, the low EE%. Moreover, the EE% of CTX in PEGNPs was not high enough, this is due to the certain solubility of CTX in aqueous media which let CTX to escape from PEGNPs [59]. Khaira et al. also showed drug contents ranged from 50 to 70% for different types of nanoparticle formulations. They found that increasing the drug polymer ratio (1:5) increased the drug content. Meanwhile the drug content could be reduced due to the polymer's separation capacity [60].

3.3. Morphological analysis using TEM

The TEM images of the CTX-PEGNPs showed that the particles were spherical in shape and that CTX was dispersed as small dark strips in the polymer matrix (Fig. 1B). However, no agglomerations were observed, and the size was 269 nm. These measurements were greater than those revealed by DLS, which indicated the particle size to be only 253.7 ± 0.3 nm [7,39,61,62]. Both methods of measurement indicated different sizes of the NPs because both methods have different sample processing steps. In the case of DLS, the hydrodynamic diameter of the particles in dispersed phase is measured, which includes a surrounding layer of the solvent. On the contrary, in TEM/scanning electron microscopy, the samples are dried, resulting in particle aggregation and consequent increase in particle size, unless the sample is monodisperse. [63].

3.4. Differential scanning calorimetry (DSC)

The thermal analysis of the pure CTX drug had an endothermic peak at 82.6 °C that began at 50.7 °C and ended at 98.5 °C; this peak due to the melting point of CTX (**S2. A)**. The endothermic peaks showed after 200 °C may due to some impurities in the raw materials. These data are agreed with our previously resorted data [7]. PEG-4000 showed an endothermic peak at 66.4 °C due to its melting point which agreed with previously reported data [46] **(S2. B)**. Pure glycerol showed an endothermic peak at 304.4 °C, which represented the melting point of glycerol (**S2. C**) [64]. CTX-PNs showed a sharp endothermic peak that began at 66.5 °C, which is related to the formulated NPs (**S2. D**). These results indicated that no physical interaction between CTX, PEG-4000, and glycerol, which confirm that the CTX-PNs can release CTX freely, moreover, the prepared CTX-PNs can be a good formula for delivery of CTX [7].

3.5. Fourier-transform infrared spectroscopy (FTIR)

FTIR of CTX showed absorption band at around 3065.25 to 3119.94 cm^{-1} is associated with the stretching vibration of (N—H and O—H). The peaks at 1553 and 1633 cm^{-1} reveal the presence of (C=C) stretching and carbonyl (C=O) groups, respectively. These results confirmed that CTX has carboxylic acid, and oxygen-containing functional groups. The peak at about 1530.48 cm^{-1} is corresponded to the stretching and bending vibration bands of N—H. Moreover, the absorption bands at 2937.1, 1423.85 and 1324 cm^{-1} can be assigned to the stretch of vibration (C—H, C=C and C—C), respectively, indicating the presence of alkyl and aryl groups [65] **(S3. A)**. The PEG-4000 displayed absorptions mainly as a result of the presence of a primary alcohol. As illustrated in **(S3. B)**, the methylene group present in PEG-4000 vibrates in the stretching mode at a frequency of 2882.14 cm^{-1}. The absorption band at 1466.21 cm^{-1} is due to binding vibration of $–CH_2$. Moreover, the primary alcohol showed the –C–O stretching vibration, a strong band around 1359.41 cm^{-1} and 1279.02 cm^{-1} [66]. The pure glycerol showed peaks of several functional groups. The O—H stretching frequency showed at 3283.31 cm^{-1}. O—H bending was observed at 1031.46 cm^{-1}, while the peak at 2932.11 and 2878.48 cm^{-1} could be attributed to C=C **(S3. C)** [67]. FTIR was used to examine the drug interaction between CTX, PEG-4000, and glycerol. Absorption bands showed no prominent interaction between the CTX, PEG-4000, and glycerol in physical mixture **(S3. D)** or formulated CTX-PNs **(S3. E)**. CTX, PEG-4000, and glycerol physical mixture showed similar absorption bands as their raw materials [36,37]. Some peaks of CTX were also disappeared in CTX-PNs absorption band which confirmed the entrapping of CTX in NPs.

3.6. Evaluation of in vitro anticancer biological activities

3.6.1. Antiproliferative activity

We compared the antiproliferative and inhibitory cytotoxic effects of CTX-PEGNPs to those of free CTX administration using an MTT assay in both lung (A549) and breast (MCF-7) cancer cell lines. The median inhibitory concentration (IC_{50}) are shown in Fig. 2A, and the cell viability values are summarized in Fig. 2B for cell line A549, and Fig. 2C for cell line MCF-7. Our results showed that CTX-PEGNPs caused dose-dependent inhibition of A549 and MCF-7 cell proliferation after 48 h

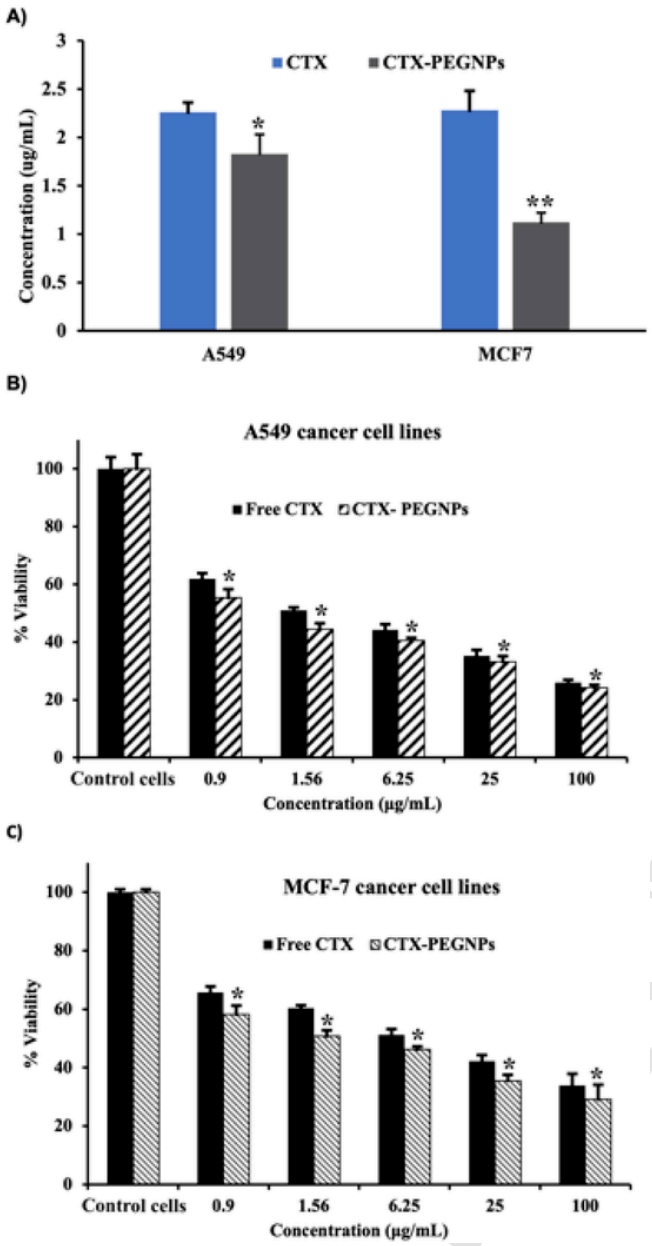

Fig. 2. Cytotoxic effects of chemotherapeutic agents on A549 and MCF-7 cell lines indicated by IC_{50} values. The cells were subjected to a treatment (48 h) with increasing concentrations of anticancer drugs (A). Cell viability of A549 (B) and MCF-7 (C) cancer cell lines treated with anticancer drugs, CTX-PEGNPs were significant in *p ≤ 0.05, **p ≤ 0.01 compared with free drug.

treatment. The results also showed differential effects of free CTX and CTX-PEGNPs on the A549 cancer cell line, with IC_{50} values of 2.26 µg/mL and 1.83 µg/mL, respectively. Furthermore, CTX-PEGNPs had a lower IC_{50} of 1.12 µg/mL in MCF-7 cells than that observed in the case of CTX alone (2.28 µg/mL). The biological features of NPs, such as cytotoxicity and cellular uptake, are significantly influenced by their surface area. Pan et al. [68] demonstrated that NPs can cause cell death via oxidative stress, and very little cytotoxicity [69]. Our findings are in line with those of Chen et al. [70] who studied the antitumor efficacy of the CTX loaded chitosan NP for drug delivery method on different cell lines and demonstrated that CTX-chitosan-NPs were significantly more effective than free drugs in inhibiting growth and proliferation. Furthermore, flow cytometry analysis of the cell cycle conducted in their study revealed that NPs had a greater capacity for intracellular uptake than free drugs administered at the same concentration, which was attributed to the co-delivery of NPs exhibiting a uniform distribution and a sustained release profile [70].

3.6.2. Gene expression in lung and breast cell lines

The results showed that the expression levels of *p21* were significantly decreased in cancer cells treated with CTX-PEGNPs, and CTX when compared with those of negative cancer cell (non-treated cell lines) (Fig. 3A). The *p21* gene is found on chromosome 6*p21*.2 and is a putative tumor suppressor gene linked to the development of a variety of cancers, including lung cancer. The protein *p21* regulates cell cycle

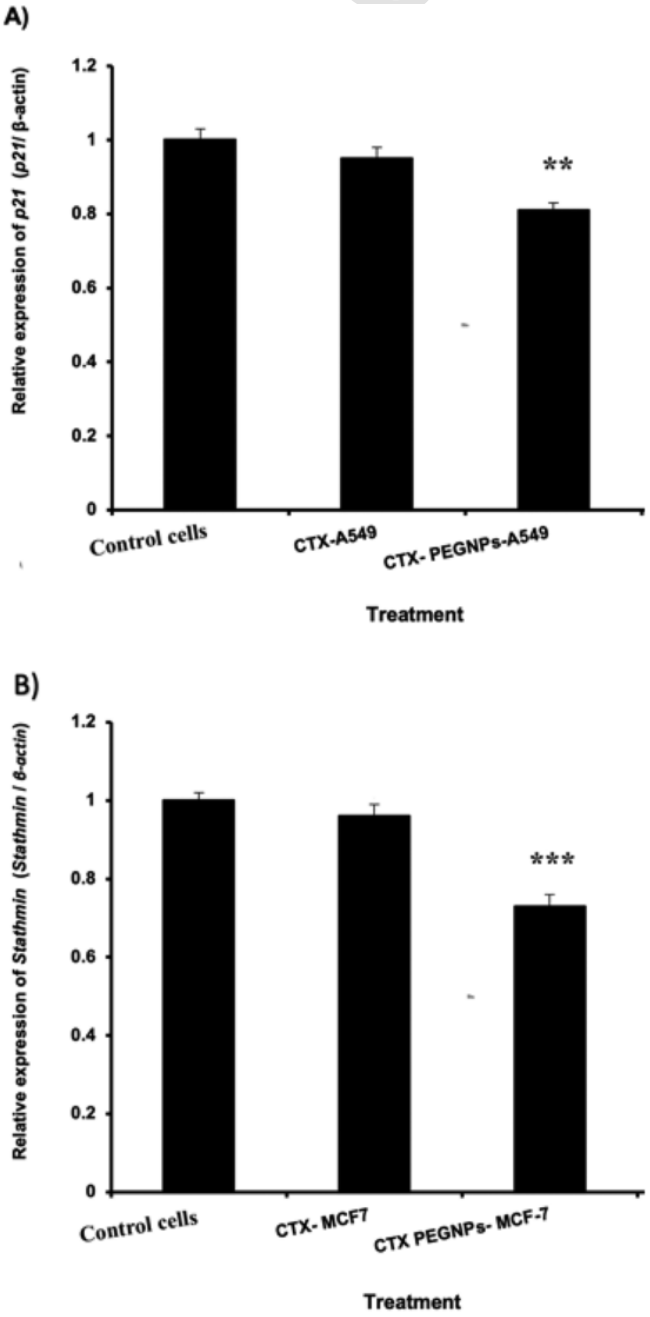

Fig. 3. (A) Effects of CTX, and CTX-PEGNPs treatment on *p21* expression in A549 and MCF-7 cell lines. Gene expression levels were standardized using the housekeeping gene *β-actin*. The data are presented as mean and standard error of the mean (SEM). (B) The change in *stathmin-1* expression in breast cancer cell line treated with CTX, and CTX-PEGNPs. Expression levels were standardized using the expression of the housekeeping gene *β-actin*. Data are presented as mean ± SEM. *$p \leq 0.05$, **$p \leq 0.01$ or ***$p \leq 0.001$ denote statistically significant differences compared with free CTX.

and apoptosis; therefore, it is a candidate for establishing molecular links between pathways that react to EGFR inhibition and CTX [71]. When DNA damage occurs, a buildup of *p21* causes the cell cycle to get arrested at the G1/S or G2/M checkpoint, allowing the cell enough time to repair the damage. This occurs through both *p53*-dependent and -independent processes [71]. We found that CTX drove the cell cycle to enter the S phase and, as a result, *p21* expression decreased. Additionally, CTX-PEGNPs downregulated *p21* expression, and the cells showed a high apoptotic rate when compared with that of the cells treated with CTX alone.

Studies on mRNA–protein relationsips have shown a poor correlation between mRNA and protein expression levels [72]. Gene transcription activity does not necessarily indicate protein synthesis. Many factors affect the relationship between these processes, such as time and the absence or availability of biological supplementary factors [72]. The *p21* protein interacts with and suppresses the transcription factor STAT3 [73], which is consistent with the hypothesis that STAT3 pathway modification by CTX-PEGNPs sensitizes the cells to EGFR inhibition. In fact, chemical suppression of the STAT3 pathway was demonstrated to promote CTX-induced apoptosis [74]. Similar results were obtained from the gene expression analysis of *stathmin-1* in MCF-7 cells; *stathmin-1* was significantly overexpressed in untreated breast cancer cells compared with CTX-PEGNP, and CTX -treated cells (Fig. 3B). Furthermore, CTX-PEGNPs demonstrated less downregulation of *p21* and *stathmin-1* in both A549 and MCF-7 cell lines than free CTX. *Stathmin-1*, also known as oncoprotein18 (Op18), is a microtubule-destabilizing protein that binds to tubulin heterodimers and modulates microtubule dynamics [23]. Microtubules function in a variety of biological activities, including cell proliferation, cell cycle progression, intracellular signal transduction, chemical transport, and cell motility. This suggests that CTX-PEGNPs can influence cytotoxicity and the expression levels of genes related to cancer progression and is a possible treatment approach for improving lung and breast cancer prognosis [23]. *Stathmin-1* expression was significantly elevated in carcinoma tissues and is negatively linked to the extent of carcinoma differentiation. *Stathmin-1* overexpression has been implicated in many human cancers, human breast cancer, and NSCLC [75,76]. Wang et al. [77] discovered *stathmin-1* overexpression in cancer cells as well, which was linked to lymph node metastases, the advanced TNM stage, and other clinical characteristics. Other *in vitro* investigations revealed that *stathmin-1* overexpression enhances cancer cell proliferation, adhesion, and metastasis, while xenograft experiments showed that *stathmin-1* overexpression enhanced mouse tumor burden and promoted cancer lung metastasis [78].

Fibronectin is a scaffolding protein that plays an important function in anaplastic cancer/tumor growth and metastasis. Silencing FAK with targeted siRNA dramatically reduced KYSE 170-STMN1 cell adhesion, invasion, and migration. This finding revealed that the degree to which *stathmin-1* promotes metastasis is dependent on increased integrin51/FAK pathway activity in cancer cells. Furthermore, the protein levels of integrin51/FAK in *stathmin-1*-silenced cells were reduced, suggesting that the activation of the integrin51/FAK pathway is regulated by the level of *stathmin-1* protein [79].

3.6.3. DNA damage in lung and breast cancer cell lines treated with CTX-PEGNPs

Single-cell gel electrophoresis, commonly known as comet assay, is used to detect DNA damage in individual eukaryotic cells. The comet assay can be applied to a wide range of medications and rapidly delivers reliable findings with minimal criteria [80]. We used comet assay to assess the response of both A549 and MCF-7 cell lines to CTX-PEGNPs and free drug treatments. These drugs had different effects on the different cancer cell types, illustrating the diversity of cancer types (Table 3:). Our findings revealed that the cells treated with CTX-PEGNPs showed the highest values of DNA damage in A549 and MCF7cell lines, with percentages of 19.25 ± 0.85% and 20.25 ± 1.12% (Table 3:), when compared with that of the cells treated with CTX alone (Figs. 4A-D), respectively. Comet assay visualization scores for (Fig. 4A) normal DNA (class 0) and damaged DNA (Class 1) and (Fig. 4B) damaged DNA (classes 2 and 3) in A549 lung cancer cell line treated with CTX-PEGNP, and CTX free drug. Comet assay visualization scores for (Fig. 4C) normal DNA (class 0) and (Fig. 4D) damaged DNA (classes 1, 2, and 3) in MCF-7 breast cancer cell line treated with CTX-PEGNPs, and CTX free drug. Comet visual scoring was determined on a five-point scale ranging from 0 to 4. In a grade-4 comet cell, all the DNA is in the "tail," whereas in a grade-0 comet cell, all the DNA is in the "head." These comet counts provided a quantitative measure for 100 cells on a scale of 0 to 4. Furthermore, a high score indicated that the cells were destroyed, with most of the DNA in the tail. A drop in the score indicated unfragmented cells [81]. Our findings are similar to those of Mirzaie et al., who reported DNA fragmentation in MCF-7 cells treated with DTX-CS-NPs, which was a characteristic morphological indication of apoptosis [82].

The uptake of CTX-PEGNPs by cells can be considerably influenced by the NP size, concentration, and cell type [50,83]. Our *in vitro* model using A549 and MCF-7 cells indicated that CTX-PEGNPs significantly increased DNA damage, which might be attributed to increased particle uptake by cells via bioadhesion, prolonged release, and EGFR-mediated endocytosis when compared to that of treatment with CTX alone. Additionally, our results are consistent with those reported by Garanti et al. who found increased cytotoxicity and DNA damage in U87 MG cells due to the increased absorption of Asiatic acid loaded with RGD-decorated solid lipid NPs [84]. In our study we confirm that the NPs of size 253 nm can internalized efficiently. Hoshyar, Gray et al. 2016 [87] reported that the NPs of size range of (30 - 500 nm) can be internalized depending on the size of particles, with larger particles having reduced internalization. Lu, Wu et al. 2009 [88] stated that the cellular uptake is considered particle-size-dependent in the order (50 > 30> 110 > 280 > 170 nm). A 50-nm NPs size was approximately taken up 2.5 times greater compared to 30-nm, 4 times with respect to 110-nm NPs, and 20 times in comparison to 280-nm NPs. Furthermore, Kulkarni and Feng 2013 [89] confirmed the higher cellular uptake efficiency of 200 nm NPs by Caco-2 and MDCK cells after 2 h incubation, compared to 500 nm NPs which showed reduced internalization and cellular uptake.

3.6.4. Measurement of DNA fragmentation in A549 and MCF7 after CTX-PEGNP treatment

Random breakage of DNA in necrotic cells results in a diffuse smear during DNA electrophoresis. Thus, DNA gel electrophoresis was applied to establish the mechanism of cell death that could be triggered by CTX-

Table 2
Rate constants and correlation coefficients for all formulations using zero-order, first-order, Higuchi, and Hixson-Crowell equations.

Brand	Zero-Order		First-Order		Higuchi Diffusion model		Hixson-Crowell	
	Release rate constant (%.hr^{-1})	r^2	Release rate constant (hr^{-1})	r^2	Release rate constant (%.hr$^{1/2}$)	r^2	Release rate constant (%$^{1/3}$.hr^{-1})	r^2
CTX-PNs	5.147	0.878	0.887	0.862	35.233	0.950	0.200	0.957
CTX	0.500	0.883	0.047	0.835	8.797	0.976	1.003	0.889

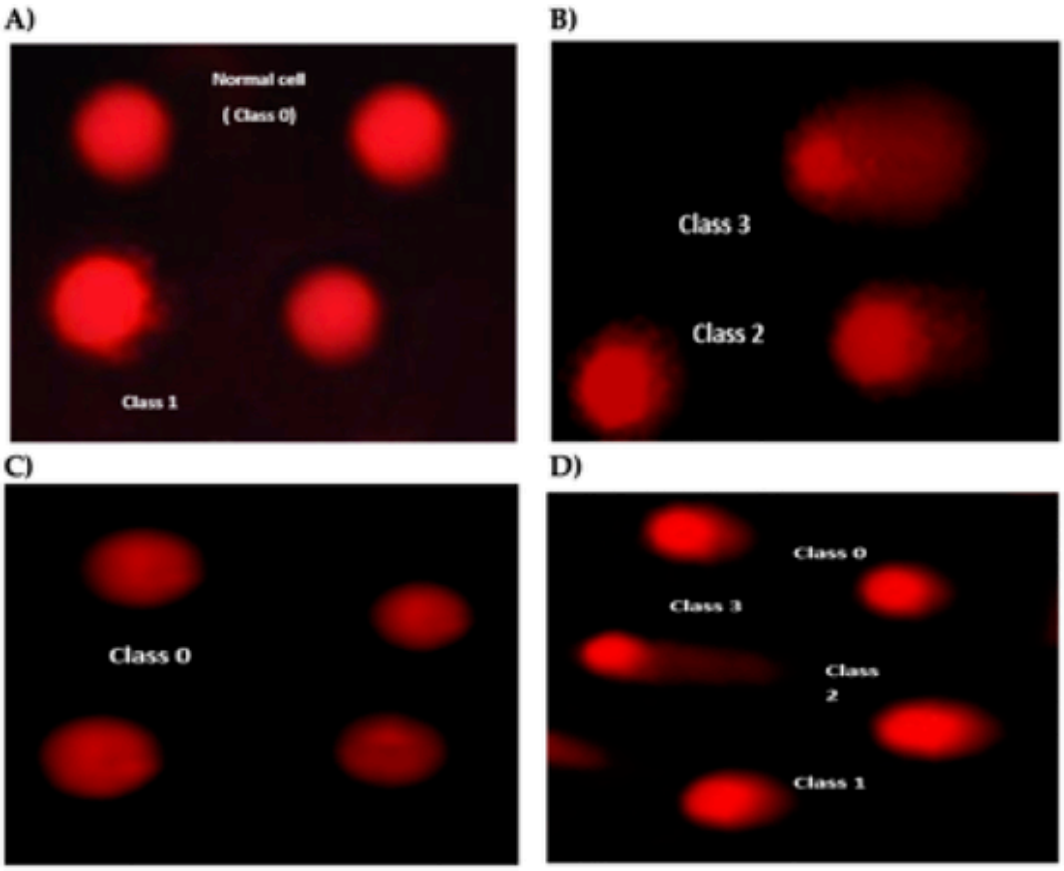

Fig. 4. Comet assay visualization scores for (A) normal DNA (class 0) and damaged DNA (Class 1) and (B) damaged DNA (classes 2 and 3) in A549 lung cancer cell line treated with CTX, CTX-PEGNP. Comet assay visualization scores for (C) normal DNA (class 0) and (D) damaged DNA (classes 1, 2, and 3) in MCF-7 breast cancer cell line treated with CTX, CTX-PEGNPs.

PEGNPs. Late apoptosis is characterized by DNA fragmentation and nuclear condensation [85].

The rates of DNA fragmentation in A549 and MCF-7 cancer cell lines are summarized in Table 4: and shown in Fig. 5A and B. The results showed that DNA fragmentation values increased significantly in both cancer cell lines when compared with that of the negative control. Moreover, the DNA fragmentation rates observed in A549 and MCF-7 cells treated with CTX-PEGNPs were 20.4 ± 0.33 and 21.5 ± 0.20, respectively, which were substantially greater than those in free CTX-treated A549 and MCF-7 cells. In our study, no ladder development was observed in untreated cells, which indicated that the cytotoxic effect of CTX-PEGNP treatment promoted the development of apoptotic DNA fragments. These results showed that the effects of the CTX-PEGNP treatment on A549 and MCF-7 cell lines were mediated by an apoptotic mechanism. Additional research is needed to investigate the biological and apoptotic effects of CTX-PEGNPs, as well as the chance of causing necrotic cell death in cancer cells. Many anticancer medicines, including cladribine, cisplatin, and 5-fluorouracil, have been demonstrated to have both apoptotic and necrotic effects. When a cell dies from necrosis, the plasma membrane loses its integrity, which allows the cytoplasmic contents to leak into the extracellular environment and produce an inflammatory response [86] (.
)

However, we have confirmed our *p21*'s qPCR data in A549 lung cancer cells & *stathmin*'s qPCR data in MCF-7 brest cancer cells using the DNA fragmentation procedure and commet assays, as we tried to double confirm that our new formula has positively impacted the expression of both genes in two different types of cancer cells, therefore, positively impacted the DNA damging and the apoptic processes as well. Thus, compared to our positive and negative control we thought the current qPCR plus DNA fragmentation & single-cell gel electrophoresis (commet assays) would be enough to prove the modified formula effect.

Table 3
Visual score of DNA damage in lung and breast tumor cell lines treated with CTX, and CTX-PEGNPs.

Treatment	No of samples	No. of cells Analyzed*	Comets	Class** 0	1	2	3	DNA damaged cells % (Mean ± SEM)
Lung tumor cell lines (A549)								
Cancer cell lines (−ve)	4	400	38	362	23	11	4	9.50 ± 1.55^{d}
CTX	4	400	53	347	31	14	8	13.27 ± 0.87^{c}
CTX-PEGNPs	4	400	77	323	27	21	29	19.25 ± 0.85^{b}
Breast tumor cell lines (MCF-7)								
Cancer cell lines (−ve)	4	400	41	359	25	10	6	10.25 ± 1.49^{d}
CTX	4	400	61	339	30	19	12	15.26 ± 1.49^{c}
CTX-PEGNPs	4	400	81	319	34	22	25	20.25 ± 1.12^{b}

*: Number of cells examined per a group, **: Class 0 = no tail; 1 = tail length < diameter of nucleus; 2 = tail length between 1× and 2× the diameter of nucleus; and 3 = tail length > 2× the diameter of nucleus. Means with different superscripts (a, b, c) between treatments in the same column are significantly different at $P < 0.05$.

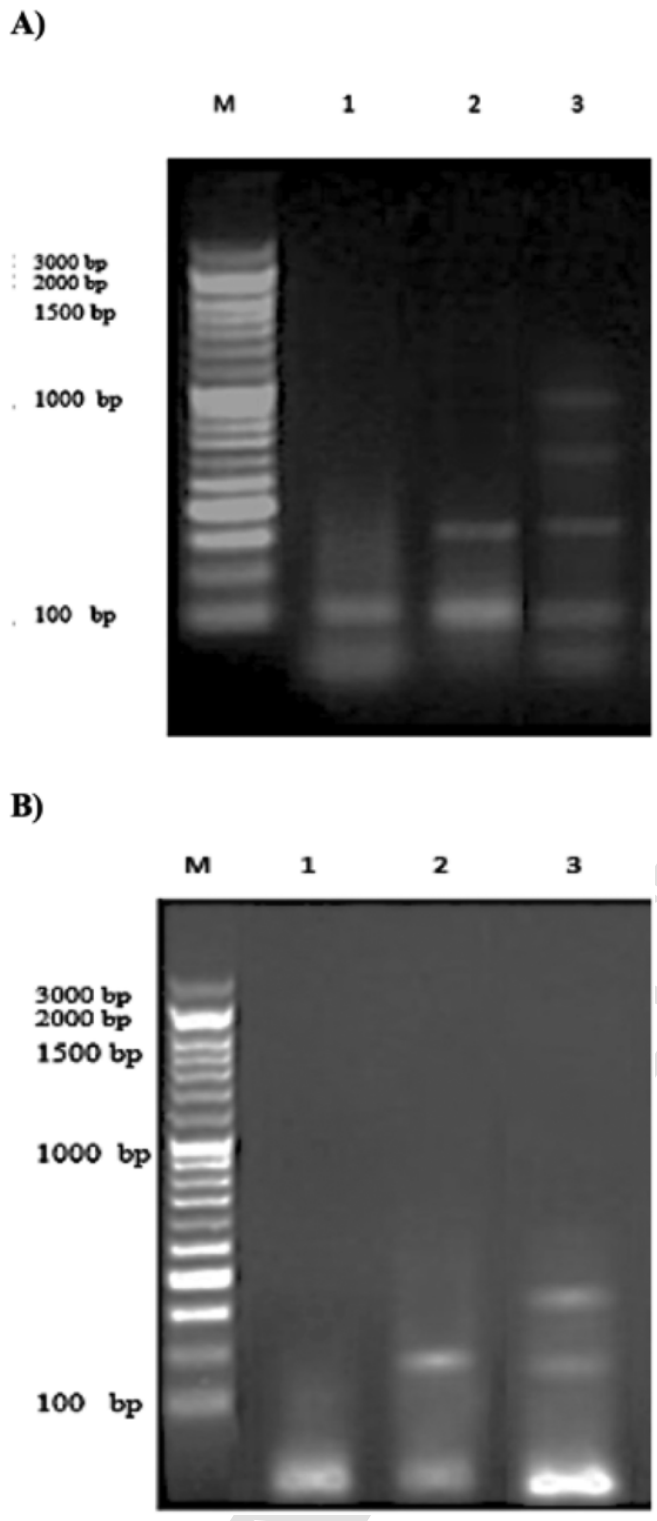

Fig. 5. Agarose gel shows the DNA fragmentation proceeded within the two used cell lines (A549/MCF-7). Each cell line has the positive, negative control and the CTX-PEGNPs formula. **A)** Show the qualitative data of DNA fragmentation in A549 lung cancer cell lines, DNA from untreated samples, Lane-1 (9.1%), Free CTX drug treated samples, Lane-2 (14.3%) and CTX-PEGNPs for 24 h, Lane-3 (20.4%), lane-M 100 bp DNA ladder marker. **B)** Show the qualitative data of DNA fragmentation in MCF-7 breast cancer cell lines, DNA from untreated samples, Lane-1 (10.2%), free CTX drug treated samples, Lane-2 (15.6%) and CTX-PEGNPs for 24 h, Lane-3 (21.5%), lane-M 100 bp DNA ladder marker.

Table 4
DNA fragmentation detected in lung and breast cancer cell lines treated with CTX, and CTX-PEGNPs.

Treatment	DNA Fragmentation % M ± SEM	Change	Inhibition
Lung breast tumor cell lines (A549)			
Cancer cell lines (−ve)	9.1 ± 0.23^{c}	0	0
CTX	14.3 ± 0.41^{b}	5.2	−62.86
CTX-PEGNPs	20.4 ± 0.33^{b}	11.3	−19.29
Breast tumor cell lines (MCF-7)			
Cancer cell lines (−ve)	10.2 ± 0.26^{c}	0	0
CTX	15.6 ± 0.25^{c}	5.4	−64.47
CTX-PEGNPs	21.5 ± 0.20^{b}	11.3	−25.65

Means with different superscripts (a, b, c) between treatments in the same column are significantly different at $P < 0.05$.

4. Conclusions

Homogeneously dispersed NPs were synthesized with acceptable size and stability and which consistently exhibited low PDI values using a simple and easily reproducible method. CTX-PEGNPs had a considerable effect on the outcomes according to the findings of both cancer cell lines. In addition, a significant downregulation of the *p21* expression in the A549 cell line and that of *stathmin-1* expression in the MCF-7 cell line was demonstrated as an important factor for cell proliferation, differentiation, and death. Furthermore, the cytotoxic effect of CTX-PEGNP treatment induced the development of apoptotic DNA fragmentation. Based on these results, additional clinical trials should be conducted to study CTX-PEGNP formulation as a potential treatment modality for different cancer types.

Funding

The authors extend their appreciation to the Deputyship for Research and Innovation, Ministry of Education, Saudi Arabia, for funding this research work through the project number (QU-IF-1-2-1). The authors also thank to the technical support of Qassim university.

Availability of data and materials

Not applicable.

CRediT authorship contribution statement

AAHA, NST, MA, IS, and ATA conceived the project. AAHA, MA, OAR, AB, and ATA curated the data. AAHA, NST, AB, IS, and ATA conducted formal analyses. AAHA acquired the funding. AAHA, MA, and ATA conducted the experimental investigation. AAHA, NST, IS, and ATA developed the methodology. AAHA, NST, and OAR performed project administration. AAHA and ATA provided resources. AB and ATA developed software. AAHA and AB supervised the project. OAR conducted imaging analyses. AAHA, NST, MA, OAR, IS, and ATA wrote the original draft of the manuscript. AAHA, AB, and ATA reviewed and edited the manuscript.

Research on human participants

No research was conducted on human participants in this study.

Declaration of competing interest

The authors declare no conflict of interest.

Acknowledgements

The researchers would like to thank the Deanship of Scientific Research, Qassim University, for supporting this project. The authors also thank Qassim University for providing technical support.

Appendix A. Supplementary data

Supplementary data to this article can be found online at https://doi.org/10.1016/j.lfs.2022.120403.

References

[1] M.M. Hou, C.L. Ho, H.Y. Lin, Y. Zhu, X. Zhang, Phase I first-in-human study of HLX07, a novel and improved recombinant anti-EGFR humanized monoclonal antibody, in patients with advanced solid cancers, Investig. New Drugs 39 (5) (2021) 1315–1323.
[2] R. Roskoski Jr., Small molecule inhibitors targeting the EGFR/ErbB family of protein-tyrosine kinases in human cancers, Pharmacol. Res. 139 (2019) 395–411.
[3] B. Vincenzi, A. Zoccoli, F. Pantano, O. Venditti, S. Galluzzo, Cetuximab: from bench to bedside, Curr. Cancer Drug Targets 10 (1) (2010) 80–95.
[4] P.H. Lin, C.L. Tseng, Y.C. Cheng, C.H. Ho, S. Chen, Y. Wang, et al., Distinguishing features of a novel humanized anti-EGFR monoclonal antibody based on cetuximab with superior antitumor efficacy, Expert. Opin. Biol. Ther. 21 (11) (2021) 1491–1507.
[5] P. Seshacharyulu, M.P. Ponnusamy, D. Haridas, M. Jain, A.K. Ganti, S.K. Batra, Targeting the EGFR signaling pathway in cancer therapy, Expert Opin. Ther. Targets 16 (1) (2012) 15–31.
[6] X. Zhang, Y. Li, M. Wei, C. Liu, T. Yu, J. Yang, Cetuximab-modified silica nanoparticle loaded with ICG for tumor-targeted combinational therapy of breast cancer, Drug Deliv. 26 (1) (2019) 129–136.
[7] A.A.H. Abdellatif, M.A. Ibrahim, M.A. Amin, H. Maswadeh, M.N. Alwehaibi, S.N. Al-Harbi, et al., Cetuximab conjugated with octreotide and entrapped calcium alginate-beads for targeting somatostatin receptors, Sci. Rep. 10 (1) (2020) 4736.
[8] S. Hornig, T. Heinze, C.R. Becer, U.S. Schubert, Synthetic polymeric nanoparticles by nanoprecipitation, J. Mater. Chem. 19 (23) (2009).
[9] U. Farghaly Aly, H.A. Abou-Taleb, A.A. Abdellatif, Tolba N. Sameh, Formulation and evaluation of simvastatin polymeric nanoparticles loaded in hydrogel for optimum wound healing purpose, Drug Des. Devel. Ther. 13 (2019) 1567–1580.
[10] A. Ghosh, P. Upadhyay, S. Sarker, S. Das, M. Bhattacharjee, S. Bhattacharya, et al., Delivery of novel coumarin-dihydropyrimidinone conjugates through mixed polymeric nanoparticles to potentiate therapeutic efficacy against triple-negative breast cancer, Biomater. Sci. 9 (16) (2021) 5665–5690.
[11] J.J. Verhoef, T.J. Anchordoquy, Questioning the use of PEGylation for drug delivery, Drug Deliv. Transl. Res. 3 (6) (2013) 499–503.
[12] S.A. Johnstone, D. Masin, L. Mayer, M.B. Bally, Surface-associated serum proteins inhibit the uptake of phosphatidylserine and poly(ethylene glycol) liposomes by mouse macrophages, Biochim. Biophys. Acta 1513 (1) (2001) 25–37.
[13] N. Dos Santos, C. Allen, A.M. Doppen, M. Anantha, K.A. Cox, R.C. Gallagher, et al., Influence of poly(ethylene glycol) grafting density and polymer length on liposomes: relating plasma circulation lifetimes to protein binding, Biochim. Biophys. Acta 1768 (6) (2007) 1367–1377.
[14] B.O. Haglund, Solubility studies of polyethylene glycols in ethanol and water, Thermochim. Acta 114 (1) (1987) 97–102.
[15] Y. Tang, Z. Li, N. He, L. Zhang, C. Ma, X. Li, et al., Preparation of functional magnetic nanoparticles mediated with PEG-4000 and application in Pseudomonas aeruginosa rapid detection, J. Biomed. Nanotechnol. 9 (2) (2013) 312–317.
[16] J.V. Jokerst, T. Lobovkina, R.N. Zare, S.S. Gambhir, Nanoparticle PEGylation for imaging and therapy, Nanomedicine (Lond.) 6 (4) (2011) 715–728.
[17] L. Fang, M. Roth, C. Teck S'ng, M. Tamm, B. Han, B.X. Hoang, Corrigendum to "Zinc salicylate reduces airway smooth muscle cells remodelling by blocking mTOR and activating p21((waf1/cip1))" [Journal of nutritional biochemistry 89 (2021) 108563], J. Nutr. Biochem. 98 (2021) 108822.
[18] L. Fang, M. Roth, C.T. S'Ng, M. Tamm, B. Han, B.X. Hoang, Zinc salicylate reduces airway smooth muscle cells remodelling by blocking mTOR and activating p21((Waf1/Cip1)), J. Nutr. Biochem. 89 (2021) 108563.
[19] W. Li, Y. Li, H. Zhang, M. Liu, H. Gong, Y. Yuan, et al., HOTAIR promotes gefitinib resistance through modification of EZH2 and silencing p16 and p21 in non-small cell lung cancer, J. Cancer 12 (18) (2021) 5562–5572.
[20] A. Efeyan, M. Collado, S. Velasco-Miguel, M. Serrano, Genetic dissection of the role of p21Cip1/Waf1 in p53-mediated tumour suppression, Oncogene 26 (11) (2007) 1645–1649.
[21] A. Marchetti, C. Doglioni, M. Barbareschi, F. Buttitta, S. Pellegrini, G. Bertacca, et al., p21 RNA and protein expression in non-small cell lung carcinomas: evidence of p53-independent expression and association with tumoral differentiation, Oncogene 12 (6) (1996) 1319–1324.
[22] W. Nie, M.D. Xu, L. Gan, H. Huang, Q. Xiu, B. Li, Overexpression of stathmin 1 is a poor prognostic biomarker in non-small cell lung cancer, Lab. Investig. 95 (1) (2015) 56–64.
[23] S. Rana, P.B. Maples, N. Senzer, J. Nemunaitis, Stathmin 1: a novel therapeutic target for anticancer activity, Expert. Rev. Anticancer. Ther. 8 (9) (2008) 1461–1470.
[24] Y. Lu, C. Liu, Y.-F. Xu, H. Cheng, S. Shi, C.-T. Wu, et al., Stathmin destabilizing microtubule dynamics promotes malignant potential in cancer cells by epithelial-mesenchymal transition, Hepatobiliary Pancreat. Dis. Int. 13 (4) (2014) 386–394.
[25] S.K. Marie, S.M. Oba-Shinjo, R. da Silva, M. Gimenez, G. Nunes Reis, J.P. Tassan, et al., Stathmin involvement in the maternal embryonic leucine zipper kinase pathway in glioblastoma, Proteome Sci. 14 (2016) 6.
[26] H.T. Tan, W. Wu, Y.Z. Ng, X. Zhang, B. Yan, C.W. Ong, et al., Proteomic analysis of colorectal cancer metastasis: stathmin-1 revealed as a player in cancer cell migration and prognostic marker, J. Proteome Res. 11 (2) (2012) 1433–1445.
[27] D. Bhagirath, N. Abrol, R. Khan, M. Sharma, A. Seth, A. Sharma, Expression of CD147, BIGH3 and stathmin and their potential role as diagnostic marker in patients with urothelial carcinoma of the bladder, Clin. Chim. Acta 413 (19–20) (2012) 1641–1646.
[28] R. Sun, Z. Liu, L. Wang, W. Lv, J. Liu, C. Ding, et al., Overexpression of stathmin is resistant to paclitaxel treatment in patients with non-small cell lung cancer, Tumour Biol. 36 (9) (2015) 7195–7204.
[29] J. Dong, M.X. Liu, Y.J. Yang, H.B. Xu, X.L. Yang, Characterization of Me. PEG-PLA copolymer nanoparticles prepared by modified spontaneous emulsion-solvent evaporation, Yao Xue Xue Bao 39 (9) (2004) 677–680.
[30] T. Higuchi, K.A. Connors, Advances in analytical chemistry and instrumentation, in: Phase solubilityStudies, 1965, pp. 117–212.
[31] F. Imanparast, M.A. Faramarzi, M. Paknejad, F. Kobarfard, A. Amani, M. Doosti, Preparation, optimization, and characterization of simvastatin nanoparticles by electrospraying: an artificial neural networks study, J. Appl. Polym. Sci. 133 (28) (2016).
[32] S. Kalimuthu, A. Yadav, Formulation and evaluation of carvedilol loaded Eudragit E 100 nanoparticles, Int. J. PharmTech Res. 1 (2) (2009) 179–183.
[33] C.A. Schneider, W.S. Rasband, K.W. Eliceiri, NIH Image to ImageJ: 25 years of image analysis, Nat. Methods 9 (7) (2012) 671–675.
[34] B.K. Satheeshababu, I. Mohamed, Synthesis and characterization of sodium alginate conjugate and study of effect of conjugation on drug release from matrix tablet, Indian J. Pharm. Sci. 77 (5) (2015) 579–585.
[35] I.B. Durowoju, K.S. Bhandal, J. Hu, B. Carpick, M. Kirkitadze, Differential scanning calorimetry — a method for assessing the thermal stability and conformation of protein antigen, J. Vis. Exp. 121 (2017).
[36] M. Nagpal, S.K. Singh, D. Mishra, Synthesis characterization and in vitro drug release from acrylamide and sodium alginate based superporous hydrogel devices, Int. J. Pharm. Investig. 3 (3) (2013) 131–140.
[37] H.Y. Zhang, W.Q. Xu, Y.Y. Zheng, E. Omari-Siaw, Y. Zhu, X. Cao, et al., Octreotide-periplocymarin conjugate prodrug for improving targetability and anti-tumor efficiency: synthesis, in vitro and in vivo evaluation, Oncotarget 7 (52) (2016) 86326–86338.
[38] L.X. Meng, Q. Ren, Q. Meng, Y.X. Zheng, M.L. He, S.Y. Sun, et al., Trastuzumab modified silica nanoparticles loaded with doxorubicin for targeted and synergic therapy of breast cancer, Artif. Cells Nanomed. Biotechnol. 46 (sup3) (2018) S556–S563.
[39] A.A.H. Abdellatif, Z. Rasheed, A.H. Alhowail, A. Alqasoumi, M. Alsharidah, R.A. Khan, et al., Silver citrate nanoparticles inhibit PMA-induced TNFalpha expression via deactivation of NF-kappaB activity in human cancer cell-lines, MCF-7, Int. J. Nanomedicine 15 (2020) 8479–8493.
[40] A.A.H. Abdellatif, M. Alsharidah, O. Al Rugaie, H.M. Tawfeek, N.S. Tolba, Silver nanoparticle-coated ethyl cellulose inhibits tumor necrosis factor-alpha of breast cancer cells, Drug Des. Devel. Ther. 15 (2021) 2035–2046.
[41] T. Mosmann, Rapid colorimetric assay for cellular growth and survival: application to proliferation and cytotoxicity assays, J. Immunol. Methods 65 (1–2) (1983) 55–63.
[42] Q. Yang, M. Feng, X. Ma, H. Li, W. Xie, Gene expression profile comparison between colorectal cancer and adjacent normal tissues, Oncol. Lett. 14 (5) (2017) 6071–6078.
[43] P. Moller, H. Stopper, A.R. Collins, Measurement of DNA damage with the comet assay in high-prevalence diseases: current status and future directions, Mutagenesis 35 (1) (2020) 5–18.
[44] A. Collins, M. Dušinská, M. Franklin, M. Somorovská, H. Petrovská, S. Duthie, et al., Comet assay in human biomonitoring studies: reliability, validation, and applications, Environ. Mol. Mutagen. 30 (2) (1997) 139–146.
[45] A. Yawata, M. Adachi, H. Okuda, Y. Naishiro, T. Takamura, M. Hareyama, et al., Prolonged cell survival enhances peritoneal dissemination of gastric cancer cells, Oncogene 16 (20) (1998) 2681–2686.
[46] M. El-Badry, G. Fetih, M. Fathy, Improvement of solubility and dissolution rate of indomethacin by solid dispersions in Gelucire 50/13 and PEG4000, Saudi Pharm. J. 17 (3) (2009) 217–225.
[47] R. Sabra, N. Billa, C.J. Roberts, Cetuximab-conjugated chitosan-pectinate (modified) composite nanoparticles for targeting colon cancer, Int. J. Pharm. 572 (2019) 118775.
[48] V. Bhaskar, R. Prakash, Devanna (Eds.), Development, Characterization and Evaluation of Simvastatin Solid Lipid Nanoparticles Loaded Transdermal Patch, 2016.
[49] M. Danaei, M. Dehghankhold, S. Ataei, F. Hasanzadeh Davarani, R. Javanmard, A. Dokhani, et al., Impact of particle size and polydispersity index on the clinical applications of lipidic nanocarrier systems, Pharmaceutics 10 (2) (2018).
[50] P. Foroozandeh, A.A. Aziz, Insight into cellular uptake and intracellular trafficking of nanoparticles, Nanoscale Res. Lett. 13 (1) (2018) 339.
[51] N.K. Rajendran, S.S.D. Kumar, N.N. Houreld, H. Abrahamse, A review on nanoparticle based treatment for wound healing, J. Drug Deliv. Sci. Technol. 44 (2018) 421–430.
[52] V.R. Shinde Patil, C.J. Campbell, Y.H. Yun, S.M. Slack, D.J. Goetz, Particle

diameter influences adhesion under flow, Biophys. J. 80 (4) (2001) 1733–1743.
[53] A. Lamprecht, U. Schafer, C.M. Lehr, Size-dependent bioadhesion of micro- and nanoparticulate carriers to the inflamed colonic mucosa, Pharm. Res. 18 (6) (2001) 788–793.
[54] M.P. Desai, V. Labhasetwar, E. Walter, R.J. Levy, G.L. Amidon, The mechanism of uptake of biodegradable microparticles in Caco-2 cells is size dependent, Pharm. Res. 14 (11) (1997) 1568–1573.
[55] Y. He, K. Park, Effects of the microparticle shape on cellular uptake, Mol. Pharm. 13 (7) (2016) 2164–2171.
[56] Z.P. Xu, M. Niebert, K. Porazik, T.L. Walker, H.M. Cooper, A.P. Middelberg, et al., Subcellular compartment targeting of layered double hydroxide nanoparticles, J. Control. Release 130 (1) (2008) 86–94.
[57] S. Muro, C. Garnacho, J.A. Champion, J. Leferovich, C. Gajewski, E.H. Schuchman, et al., Control of endothelial targeting and intracellular delivery of therapeutic enzymes by modulating the size and shape of ICAM-1-targeted carriers, Mol. Ther. 16 (8) (2008) 1450–1458.
[58] A.H. Ranneh, Y. Iwao, S. Noguchi, T. Oka, S. Itai, The use of surfactants to enhance the solubility and stability of the water-insoluble anticancer drug SN38 into liquid crystalline phase nanoparticles, Int. J. Pharm. 515 (1–2) (2016) 501–505.
[59] K.M. El-Say, Maximizing the encapsulation efficiency and the bioavailability of controlled-release cetirizine microspheres using Draper-Lin small composite design, Drug Des. Devel. Ther. 10 (2016) 825–839.
[60] R. Khaira, J. Sharma, V. Saini, Development and characterization of nanoparticles for the delivery of gemcitabine hydrochloride, ScientificWorldJournal 2014 (2014) 560962.
[61] A.A.H. Abdellatif, R. Hennig, K. Pollinger, H.M. Tawfeek, A. Bouazzaoui, A. Goepferich, Fluorescent nanoparticles coated with a somatostatin analogue target blood monocyte for efficient leukaemia treatment, Pharm. Res. 37 (11) (2020) 217.
[62] A.A.H. Abdellatif, A plausible way for excretion of metal nanoparticles via active targeting, Drug Dev. Ind. Pharm. 46 (5) (2020) 744–750.
[63] R. Mitra, S. Bhattacharya, Inhibition in binding between fullerene and a bisporphyrin in presence of silver nanoparticles in solution: UV-Vis, DLS, SEM and TEM studies, Spectrochim. Acta A Mol. Biomol. Spectrosc. 114 (2013) 11–18.
[64] E.A. Arık Kibar, F. Us, Thermal, mechanical and water adsorption properties of corn starch–carboxymethylcellulose/methylcellulose biodegradable films, J. Food Eng. 114 (1) (2013) 123–131.
[65] H. Su, Y. Liao, F. Wu, X. Sun, H. Liu, K. Wang, et al., Cetuximab-conjugated iodine doped carbon dots as a dual fluorescent/CT probe for targeted imaging of lung cancer cells, Colloids Surf. B Biointerfaces 170 (2018) 194–200.
[66] K.U. Khan, M.U. Minhas, M. Sohail, S.F. Badshah, O. Abdullah, S. Khan, et al., Synthesis of PEG-4000-co-poly (AMPS) nanogels by cross-linking polymerization as highly responsive networks for enhancement in meloxicam solubility, Drug Dev. Ind. Pharm. 47 (3) (2021) 465–476.
[67] N.A. Razali, M. Conte, J. McGregor, The role of impurities in the La2O3 catalysed carboxylation of crude glycerol, Catal. Lett. 149 (5) (2019) 1403–1414.
[68] Y. Pan, A. Leifert, D. Ruau, S. Neuss, J. Bornemann, G. Schmid, et al., Gold nanoparticles of diameter 1.4 nm trigger necrosis by oxidative stress and mitochondrial damage, Small 5 (18) (2009) 2067–2076.
[69] M.Y. Lan, Y.B. Hsu, C.H. Hsu, C.Y. Ho, J.C. Lin, S.W. Lee, Induction of apoptosis by high-dose gold nanoparticles in nasopharyngeal carcinoma cells, Auris Nasus Larynx 40 (6) (2013) 563–568.
[70] J. Chen, X. Yang, L. Huang, H. Lai, C. Gan, X. Luo, Development of dual-drug-loaded stealth nanocarriers for targeted and synergistic anti-lung cancer efficacy, Drug Deliv. 25 (1) (2018) 1932–1942.
[71] T. Abbas, A. Dutta, p21 in cancer: intricate networks and multiple activities, Nat. Rev. Cancer 9 (6) (2009) 400–414.
[72] A. Koussounadis, S.P. Langdon, I.H. Um, D.J. Harrison, V.A. Smith, Relationship between differentially expressed mRNA and mRNA-protein correlations in a xenograft model system, Sci. Rep. 5 (2015) 10775.
[73] O. Coqueret, H. Gascan, Functional interaction of STAT3 transcription factor with the cell cycle inhibitor p21WAF1/CIP1/SDI1, J. Biol. Chem. 275 (25) (2000) 18794–18800.
[74] C. Zhao, H. Li, H.J. Lin, S. Yang, J. Lin, G. Liang, Feedback activation of STAT3 as a cancer drug-resistance mechanism, Trends Pharmacol. Sci. 37 (1) (2016) 47–61.
[75] S.H. Wei, F. Lin, X. Wang, P. Gao, H.Z. Zhang, Prognostic significance of stathmin expression in correlation with metastasis and clinicopathological characteristics in human ovarian carcinoma, Acta Histochem. 110 (1) (2008) 59–65.
[76] L. Gan, K. Guo, Y. Li, X. Kang, L. Sun, H. Shu, et al., Up-regulated expression of stathmin may be associated with hepatocarcinogenesis, Oncol. Rep. 23 (4) (2010) 1037–1043.
[77] S. Wang, J. Akhtar, Z. Wang, Anti-STMN1 therapy improves sensitivity to antimicrotubule drugs in esophageal squamous cell carcinoma, Tumour Biol. 36 (10) (2015) 7797–7806.
[78] Q. Jiang, Y. Pan, Y. Cheng, H. Li, D. Liu, H. Li, Lunasin suppresses the migration and invasion of breast cancer cells by inhibiting matrix metalloproteinase-2/-9 via the FAK/Akt/ERK and NF-kappaB signaling pathways, Oncol. Rep. 36 (1) (2016) 253–262.
[79] P. Vitorino, S. Yeung, A. Crow, J. Bakke, T. Smyczek, K. West, et al., MAP4K4 regulates integrin-FERM binding to control endothelial cell motility, Nature 519 (7544) (2015) 425–430.
[80] N.P. Singh, M.T. McCoy, R.R. Tice, E.L. Schneider, A simple technique for quantitation of low levels of DNA damage in individual cells, Exp. Cell Res. 175 (1) (1988) 184–191.
[81] P.L. Olive, J.P. Banath, The comet assay: a method to measure DNA damage in individual cells, Nat. Protoc. 1 (1) (2006) 23–29.
[82] Z.H. Mirzaie, S. Irani, R. Mirfakhraie, S.M. Atyabi, M. Dinarvand, R. Dinarvand, et al., Docetaxel-chitosan nanoparticles for breast cancer treatment: cell viability and gene expression study, Chem. Biol. Drug Des. 88 (6) (2016) 850–858.
[83] J. Yue, T.J. Feliciano, W. Li, A. Lee, T.W. Odom, Gold nanoparticle size and shape effects on cellular uptake and intracellular distribution of siRNA nanoconstructs, Bioconjug. Chem. 28 (6) (2017) 1791–1800.
[84] T. Garanti, M.A. Alhnan, K.W. Wan, RGD-decorated solid lipid nanoparticles enhance tumor targeting, penetration and anticancer effect of asiatic acid, Nanomedicine (Lond.) 15 (16) (2020) 1567–1583.
[85] S. Samarghandian, J.T. Afshari, S. Davoodi, Chrysin reduces proliferation and induces apoptosis in the human prostate cancer cell line pc-3, Clinics (Sao Paulo) 66 (6) (2011) 1073–1079.
[86] X. Wang, S.W. Ryter, C. Dai, Z.L. Tang, S.C. Watkins, X.M. Yin, et al., Necrotic cell death in response to oxidant stress involves the activation of the apoptogenic caspase-8/bid pathway, J. Biol. Chem. 278 (31) (2003) 29184–29191.
[87] Hoshyar N, Gray S, Han H, Bao G, The effect of nanoparticle size on in vivo pharmacokinetics and cellular interaction, Nanomedicine (Lond) 11 (6) (2016) 673–692.
[88] Lu F, Wu SH, Hung Y, Mou CY, Size effect on cell uptake in well-suspended, uniform mesoporous silica nanoparticles, Small 5 (12) (2009) 1408–1413.
[89] Kulkarni SA, Feng SS, Effects of particle size and surface modification on cellular uptake and biodistribution of polymeric nanoparticles for drug delivery, Pharm Res 30 (10) (2013) 2512–2512.